Optical Engineering

OpticalEngineering.SPIEDigitalLibrary.org

High-efficiency calibration of star sensor based on two-dimensional Dammann grating

Kun Zhang
Xing Zhong
Wei Wang
Yao Meng
Chi Ma

SPIE.

Kun Zhang, Xing Zhong, Wei Wang, Yao Meng, Chi Ma, "High-efficiency calibration of star sensor based on two-dimensional Dammann grating," *Opt. Eng.* **58**(8), 085104 (2019), doi: 10.1117/1.OE.58.8.085104.

High-efficiency calibration of star sensor based on two-dimensional Dammann grating

Kun Zhang,[a,b,c] Xing Zhong,[a,b,c,*] Wei Wang,[a,b,c] Yao Meng,[c] and Chi Ma[c]
[a]Chinese Academy of Sciences, Changchun Institute of Optics, Fine Mechanics and Physics, Changchun, China
[b]University of Chinese Academy of Sciences, Beijing, China
[c]Chang Guang Satellite Technology Co., Ltd., Changchun, China

Abstract. Aiming to address the low efficiency of the traditional calibration method for star sensors, we propose a calibration method using two-dimensional (2-D) Dammann grating, which can generate a dot array with uniform intensity and a certain interval. This method is based on theoretical analysis of the diffraction angles of 2-D Dammann grating relative to the tilt angles of incident light. We calculate the angles using a fitting method and further calculate the geometric parameters, such as principal point and principal distance of the star sensor. Finally, we establish a calibration system using 2-D Dammann grating and a nanostar sensor with a 25-mm focal length and 15-deg full field of view has been calibrated. The results show that the calibration accuracy for single-star measurement is better than 6 arc sec, which satisfies the requirement for high-efficiency star sensor calibration and validates the proposed method.
[DOI: 10.1117/1.OE.58.8.085104]

Keywords: star sensor; high-efficiency calibration; Dammann grating; diffraction.

Paper 190297 received Mar. 15, 2019; accepted for publication Jul. 31, 2019; published online Aug. 19, 2019.

1 Introduction

A star sensor images stars and provides the three-axis attitude information of the carrier in the celestial coordinate system.[1,2] It is an attitude-fixing device with highest accuracy in spacecraft measurement and has currently been widely used in civilian and military applications.

The single-star measurement accuracy of star sensors determines the measurement accuracy of attitude. Therefore, calibration of star sensors is indispensable to improve their measurement accuracy, which involves evaluation of physical parameters, such as the principal point, principal distance, and distortion. Traditional ground static calibration uses a high-precision turning table calibration method, which collects the target points on the image surface of the star sensor using a turning table.[3] However, the calibration devices are expensive and the calibration process is complex, time-consuming, and largely affected by the environment.[4,5] Dynamic calibration uses a star simulator to simulate the stars in the sky to calibrate the star sensor. However, this calibration method has low precision,[6,7] and the manufacturing process of the dynamic star simulator is complex and expensive.[8,9]

One-dimensional (1-D) Dammann grating can only produce a 1-D diffraction array with equal intensity.[10] For instance, a 1-D Dammann grating with beam splitting ratio of 1×11 was designed by the genetic algorithm in Ref. 10. However, in the process of star sensor calibration, the diffraction array of Dammann grating is needed to cover the whole detector. Therefore, the diffraction array of 1-D Dammann grating does not meet the requirement. It is necessary to use two-dimensional (2-D) Dammann grating, which is obtained by 2-D orthogonalization of 1-D Dammann grating, to generate a 2-D diffraction array with equal intensity.

Aiming to address the above-mentioned shortcomings of the static and dynamic calibration methods for star sensors, a calibration method based on a 2-D Dammann grating is proposed in this paper. The 2-D Dammann grating used in the calibration is simple in structure and low-cost. Moreover, the calibration process is simple and unaffected by the environment. Calibration of the star sensor can be accomplished using the images collected at one exposure time. In this study, the calibration setup is established and a star sensor is calibrated using the proposed technique. The results show that the maximum error of a single-star measurement is <6 arc sec.

2 Research on Star Sensor Calibration Based on 2-D Dammann Grating

2.1 *Analysis of Diffraction Characteristics of 2-D Dammann Grating*

Dammann grating is a kind of binary phase grating with a periodically distributed phase structure, compared with the amplitude Dammann grating, the phase Dammann grating has higher diffraction efficiency.[11] The Fraunhofer diffraction pattern generated by 2-D Dammann grating has a certain number of 2-D equal-intensity light spots. The diffraction angle of each light spot is closely related to the direction of the incident light and the structure of the 2-D Dammann grating.

Multidirectional parallel light is generated by the diffraction of 2-D Dammann grating to simulate multiple stars at infinity. This is necessary to accurately calculate the diffraction angles of each diffraction order, which were analyzed in this study.[12,13]

When the incident light wave is a plane wave with a uniform intensity distribution and perpendicular incidence on the surface of a 2-D Dammann grating, the diffraction direction vector of the (m, n)-order is

*Address all correspondence to Xing Zhong, E-mail: ciomper@163.com

0091-3286/2019/$28.00 © 2019 SPIE

$$\mathbf{d} = [\lambda f_x, \lambda f_y, \sqrt{1-(\lambda f_x)^2-(\lambda f_y)^2}],$$
$$f_x = \frac{m}{d_x}, \quad f_y = \frac{n}{d_y}, \tag{1}$$

where f_x and f_y denote the spatial frequencies encoded in the 2-D Dammann grating, λ is the wavelength of the incident laser beam, d_x and d_y denote the grating constants, and m and n denote the particular diffraction orders. The angle between the diffraction direction of the (m, n)-order and optical axis is given by

$$\theta_{mn} = \arccos\sqrt{1-(\lambda f_x)^2-(\lambda f_y)^2}. \tag{2}$$

However, it is difficult to avoid the slight tilt of the 2-D Dammann grating with respect to the incident beam; hence, Eq. (1) is only valid if the incident light wave is a plane wave with a uniform intensity distribution and is perfectly perpendicular to the 2-D Dammann grating surface. Therefore, a more detailed analysis has been performed considering that the incident parallel light is not strictly perpendicular to the 2-D Dammann grating surface.[14,15] The 2-D Dammann grating coordinate system has been used, in which the incident beam is represented as

$$\begin{pmatrix} r_x \\ r_y \\ r_z \end{pmatrix} = \begin{pmatrix} \sin\beta \\ -\cos\beta\sin\alpha \\ \cos\beta\cos\alpha \end{pmatrix}, \tag{3}$$

with the Euler angles α and β denoting the rotation of the x and y axes, respectively, of the 2-D Dammann grating coordinate frame with respect to the collimator coordinate frame, as shown in Fig. 1. φ is the 2-D Dammann grating clocking error (in rotation around the z axis). The diffraction direction of the (m, n)-order can be obtained as follows:[16,17]

$$\begin{pmatrix} X \\ Y \\ Z \end{pmatrix} = \begin{bmatrix} \lambda f_x + r_x + (\lambda f_y + r_y)\times\sin\varphi \\ (\lambda f_y + r_y)\times\cos\varphi \\ \sqrt{1-(X^2+Y^2)} \end{bmatrix}. \tag{4}$$

Therefore, the directions of the diffracted light at all orders can be calculated from α, β, and φ. Based on Eq. (4), the angle between the diffraction direction of the (m, n)-order and the optical axis is given by

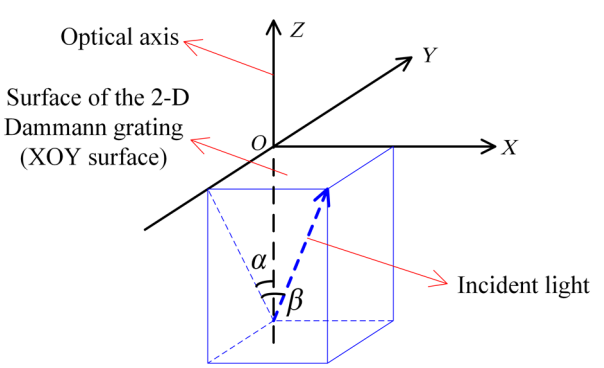

Fig. 1 Oblique incidence of the incident light.

$$\theta_{mn} = \arccos\sqrt{1-(X^2+Y^2)}. \tag{5}$$

2.2 *Design of 2-D Dammann Grating*

When the parameters of the 2-D Dammann grating are determined, the 2-D diffraction dots array must satisfy the following conditions:

1. The 2-D Dammann grating diffraction dots array must cover the full field of view of star sensors.
2. The number of dots within the full field of view of the star sensor should be as large as possible.

In this study, a nanostar sensor with a pixel size of 5.4 μm × 5.4 μm, focal length of 25 mm, and full field of view of 15 deg is calibrated. In order to obtain sufficient control points in the full field of view of the nanostar sensor and make full use of the equal-intensity diffraction orders, a 2-D Dammann grating with a dots array of 23 × 23 is selected and the grating constant is calculated using the grating equation [Eq. (6)]. When using a He–Ne laser as the light source, the grating constant of the 2-D Dammann grating should be <53.329 μm; hence, the grating constant used in the calibration experiment is 53 μm. The structure of the 2-D Dammann grating used in this study is presented in Fig. 2.[17] The black areas indicate opaqueness, whereas the gray areas indicate light transmission.[10,18] The normalized coordinates of the 2-D Dammann grating are optimized using a simulated annealing algorithm. There are six pairs of coordinate points in one cycle of the 2-D Dammann grating,[11] the total diffraction efficiency is 82.83% and the relative uniformity error of the diffraction light energy is

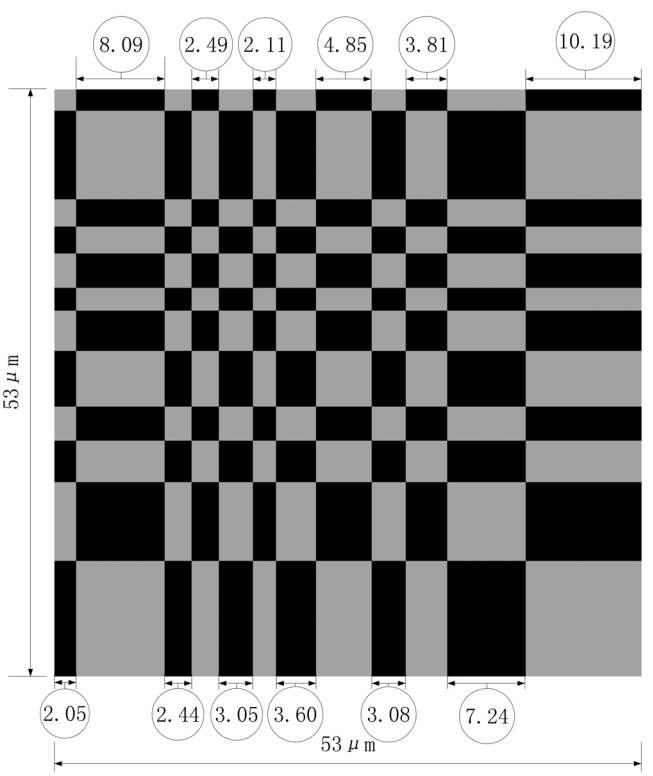

Fig. 2 Structure of the 2-D Dammann grating.

0.931%, which is an advantageous to improve the extraction accuracy of centroids. The relative uniformity error is defined in Eq. (7):

$$d \sin \theta = m\lambda, \tag{6}$$

$$\mathrm{rms} = \frac{I_{\max} - I_{\min}}{I_{\max} + I_{\min}}, \tag{7}$$

where $I_{\max}$ and $I_{\min}$ represent the maximum and minimum intensities of the required diffraction order, respectively.

However, when the grating is processed into an amplitude Dammann grating, the (0, 0)-order diffraction light will become stronger, which will lead to the saturation of the detector. In order to acquire the (0, 0)-order image point without saturation phenomenon, the transmittance of the neutral filter will be controlled. Finally, the complete image is obtained by image processing.

According to Eq. (6), the diffraction angle of the grating is closely related to the grating constant. Therefore, in order to ensure the accuracy of the grating diffraction angle and the calibration accuracy of the star sensor, the grating constant of the 2-D Dammann grating should be controlled within several nanometers. Equation (8) shows the relationship between the grating constant error and diffraction angle error:

$$\Delta\theta = \arcsin\frac{m\lambda}{d} - \arcsin\frac{m\lambda}{d + \Delta d}, \tag{8}$$

where $\Delta\theta$ is the diffraction angle error and Δd is the grating constant error.

In the calibration process of the star sensor, vignetting cannot occur in the full field of view of the star sensor. Therefore, the effective aperture size of the 2-D Dammann grating must be matched with the relevant parameters of the star sensor, and the corresponding expression is given by

$$D = D_{\mathrm{ep}} + 2L_{\mathrm{ep}} \tan(\mathrm{FOV}), \tag{9}$$

where L_{ep} is the distance between the 2-D Dammann grating, D is the effective diameter of the 2-D Dammann grating, D_{ep} is the diameter of the entrance pupil of the star sensor, and FOV denotes the half-field angle of the star sensor. The effective length of the 2-D Dammann grating in this study is 59 mm, which is much larger than the required width.

2.3 *Calibration Method*

2.3.1 *Calibration of principal point and principal distance*

In order to avoid the system errors caused by machining and adjusting, calibration is a necessary step in the development of star sensors.[19,20] In this paper, a circle fitting method is proposed to determine the principal point of the star sensor. Furthermore, the tilt angles α and β of the incident light relative to the 2-D Dammann grating are obtained from the principal point of the star sensor and the imaging point of the (0, 0)-order.

Principal point calibration method. The star sensor is fixed on a turning table. A beam of parallel light passes through the star sensor and focuses on a point in the focal plane. The star sensor is rotated gradually along the optical axis by 360 deg, and an approximate ring composed of imaging points is obtained. The obtained approximate circle is fitted with a standard circle, and the center of the fitting circle is the principal point.

In order to obtain high-accuracy tilt angle of the incident light relative to the 2-D Dammann grating, the tilt angles α and β of the incident light are obtained based on the principal point of the star sensor and the imaging point of the (0, 0)-order. During the experiment, the imaging spot of the (0, 0)-order in the captured image is collected as close as possible to the principal point, and the centroid of the imaging spot of the (0, 0)-order is extracted. The tilt angles α and β of the incident light can be calculated using the following equations:

$$\alpha = \arctan\frac{y_{00} - y_0}{f'}, \tag{10}$$

$$\beta = \arctan\frac{x_{00} - x_0}{\sqrt{f'^2 + (y_{00} - y_0)^2}}, \tag{11}$$

where (x_{00}, y_{00}) denotes the centroid coordinate of the spot of the (0, 0)-order, (x_0, y_0) denotes the principal point of the star sensor, and f' is the focal length of the star sensor.

Substituting the tilt angles α and β of the incident light into Eq. (12), the diffraction angle of the (m, n)-order can be obtained. Each control point obtained from the entire image surface of the star sensor is then substituted into Eq. (13), and the principal distance is calculated by the least-squares method:

$$\theta_{mn} = \arccos\sqrt{1 - (\lambda f_x + \sin\beta)^2 - (\lambda f_y - \cos\beta \sin\alpha)^2}, \tag{12}$$

$$\tan\theta_{mn} = \frac{\sqrt{(x_{mn} - x_0)^2 + (y_{mn} - y_0)^2}}{f}, \tag{13}$$

where f is the principal distance of the star sensor.

2.3.2 *Distortion correction*

In a practical setup, the X and Y axes of the 2-D Dammann grating are not exactly parallel to those of the star sensor focal plane. Therefore, the 2-D Dammann grating has a rotation angle around the optical axis. The $(m, 0)$ diffraction orders of the 2-D Dammann grating are imaged in a straight line by the ideal optical system. However, because of the error of centroid extraction and the aberrations of the star sensor optical system, the imaging points are not located on a straight line. A straight-line fitting method is proposed in this study to resolve the rotation angle issue.

The ideal coordinates of the 2-D Dammann grating diffraction orders on the focal plane of the star sensor are as follows:

$$\begin{pmatrix} x_{mn0} \\ y_{mn0} \end{pmatrix} = \begin{pmatrix} fX/Z \\ fY/Z \end{pmatrix}. \tag{14}$$

Therefore, in the 2-D Dammann grating calibration, the distortion at the control point (x_{mn}, y_{mn}) of the star sensor can be calculated using

$$\begin{pmatrix} \delta x_{mn} \\ \delta y_{mn} \end{pmatrix} = \begin{pmatrix} \cos\gamma & -\sin\gamma \\ \sin\gamma & \cos\gamma \end{pmatrix} \begin{pmatrix} x_{mn0} - x_0 \\ y_{mn0} - y_0 \end{pmatrix} + \begin{pmatrix} x_0 \\ y_0 \end{pmatrix} - \begin{pmatrix} x_{mn} \\ y_{mn} \end{pmatrix}, \tag{15}$$

where γ is the rotation angle of the Dammann grating around the optical axis of the star sensor.

During the processing and adjustment process, the star sensor cannot be completely ideal, and as a result, the distortion of the full field of view of the star sensor is not symmetrically distributed about the principal point. The fitting accuracy will be severely reduced if a quadratic polynomial fitting is used in the full field of view of the star sensor.

Therefore, in order to improve the accuracy of the fitting of the full field of view, in the star sensor distortion calibration, the star sensor imaging plane is divided into nine regions of equal size and the distortion data of each region are fitted with a quadratic polynomial,[21,22] as shown in Eq. (16). The residual distortion vector of each control point is calculated using Eq. (17), and the angular error corresponding to the residual distortion of each control point can be calculated using Eq. (18):

$$\begin{pmatrix}\delta x_{mn}\\ \delta y_{mn}\end{pmatrix} = \begin{pmatrix}a_1 + b_1 x_{mn} + c_1 y_{mn} + d_1 x_{mn} y_{mn} + e_1 x_{mn}^2 + f_1 y_{mn}^2\\ a_2 + b_2 x_{mn} + c_2 y_{mn} + d_2 x_{mn} y_{mn} + e_2 x_{mn}^2 + f_2 y_{mn}^2\end{pmatrix}, \tag{16}$$

$$\begin{pmatrix}\delta x'_{mn}\\ \delta y'_{mn}\end{pmatrix} = \begin{pmatrix}\delta x_{mn}\\ \delta y_{mn}\end{pmatrix} - \begin{pmatrix}a_1 + b_1 x_{mn} + c_1 y_{mn} + d_1 x_{mn} y_{mn} + e_1 x_{mn}^2 + f_1 y_{mn}^2\\ a_2 + b_2 x_{mn} + c_2 y_{mn} + d_2 x_{mn} y_{mn} + e_2 x_{mn}^2 + f_2 y_{mn}^2\end{pmatrix}, \tag{17}$$

$$\sigma = \frac{\sqrt{\delta x_{mn}'^2 + \delta y_{mn}'^2}}{\sqrt{f^2 + x_{mn}^2 + y_{mn}^2}}. \tag{18}$$

3 Experiment and Analysis

3.1 *Calibration Experiment*

The calibration setup of the star sensor is presented in Fig. 3. The light intensity of a He–Ne laser (HNL008R, Thorlabs) is largely attenuated using a neutral density filter (GCBZ-125C, Daheng Optics) to avoid saturation of the detector. The attenuated He–Ne laser is filtered using a 25-μm three-axis spatial filter at the focus of a 40× microscope objective (GCO-0112M, Daheng Optics). The laser beam is collimated by a 400-mm achromatic lens (AC508-400-B, Thorlabs). The exact position and orientation of the collimator are determined by the parallel interference fringes produced by a shear plate collimator (SI254, Thorlabs). The attenuated and collimated laser beam is incident on the surface of the 2-D Dammann grating, and each diffraction order of the grating is then imaged in the focal plane of the star sensor. The experimental images are collected in a dark room to avoid the interference caused by stray light.

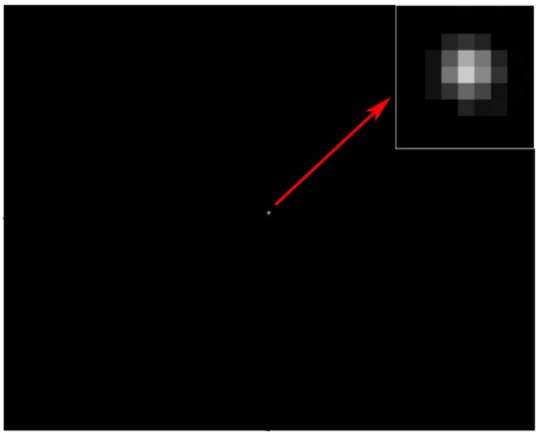

Fig. 4 (0, 0)-order diffracted light imaging point.

The polarization of the beam will barely influence the relative uniformity of all the diffraction orders; it only influences the total diffraction efficiency.[23] The energy of the He–Ne laser is very strong, in order to avoid imaging saturation of the detector, a neutral filter is needed in the experimental optical path. So the decrease of the grating diffraction efficiency will not affect the calibration of star sensor.

In the experiment, by appropriately reducing the transmittance of the neutral density filter, the (0, 0)-order diffracted light is imaged on the star sensor focal plane with moderate brightness, and the rest of the diffracted lights are attenuated, i.e., the (0, 0)-order diffracted light replaces the single-star simulator. The star sensor is rotated gradually by 360 deg and 30 images corresponding to each rotation angle are collected as shown in Fig. 4. By appropriately increasing the transmittance of the neutral density filter, the brightness at the 23×23 diffraction imaging points can be made moderate, and then 30 images are collected to reduce the random

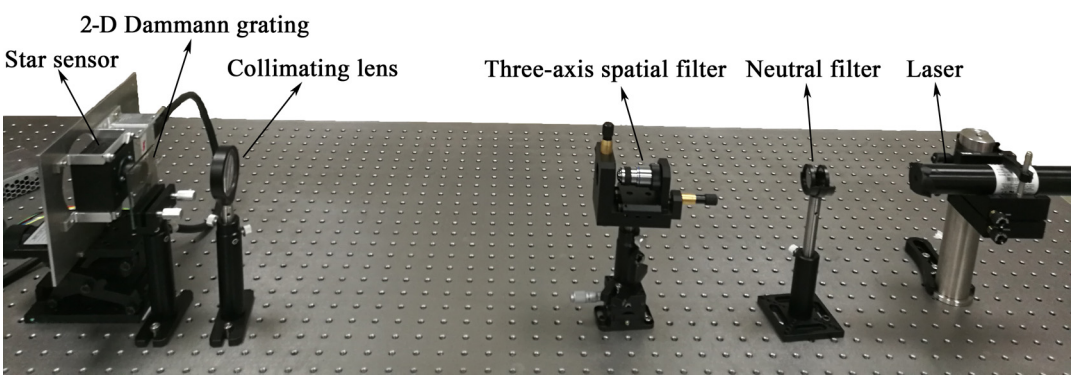

Fig. 3 Image of the calibration setup with the 2-D Dammann grating.

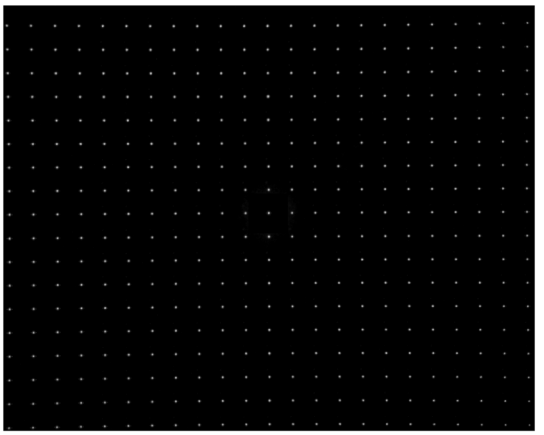

Fig. 5 Calibration grids produced by the 2-D Dammann grating.

errors produced in the experiment. The captured images are processed using a threshold, as shown in Fig. 5.

3.2 *Processing and Analysis of Experimental Data*

The centroids of the imaging points are extracted using a gray centroid algorithm.[24–27] The coordinates of each control point are the average values of multiple frames. The (0, 0)-order imaging points in the images captured by the star sensor rotated gradually by 360 deg along the optical axis are extracted, and the extracted centroids are fitted with a standard circle. The center of the fitted circle is the principal point, and the final coordinate of the principal point is (639.72, 500.73). After the centroid extraction of the 23×23 dot matrix obtained by one imaging, the incident angle of the parallel light can be obtained using Eqs. (10) and (11). Then the coordinates of the 23×23 dots array are substituted into Eq. (13) to fit the principal distance. The star sensor calibration results are presented in Table 1.

By fitting the imaging points of the $(m, 0)$-orders of the 2-D Dammann grating, the issue with the rotation angle of the 2-D Dammann grating around the optical axis is resolved and the fitting line is plotted in Fig. 6. Then the distortion at each control point of the star sensor is calculated using Eq. (15) and the distortion vectors of each control point is presented in Fig. 7.

From Fig. 7, we can see that the distortion vectors on the left side are much larger than those on the right side. This is because the processing and adjustment of the star sensor cannot be completely ideal. For example, the lens has eccentricity, tilt, and radius machining errors during processing. Moreover, there are also eccentricity, tilt, and lens-to-lens spacing errors during the assembly process. These errors will lead to asymmetrical distortion of the star sensor about the principal point; therefore, the distortion vectors on the left side are much larger than those on the right side in Fig. 7.

Table 1 Calibration results for the star sensor.

Principal point (pixels)	Principal distance (pixels)	α (deg)	β (deg)
(639.72, 500.73)	4698.18	0.0025	0.0102

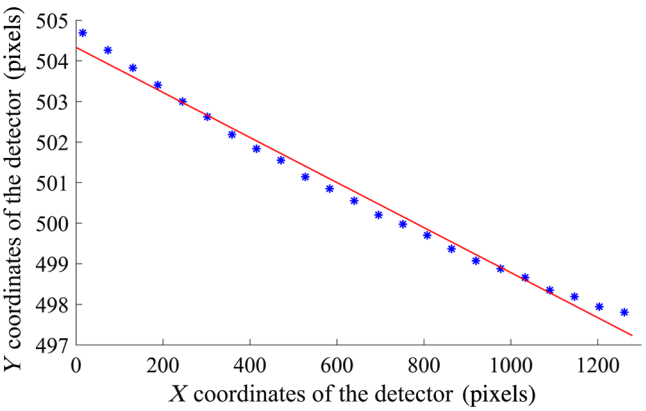

Fig. 6 Fitting line diagram of the $(m, 0)$-order control points.

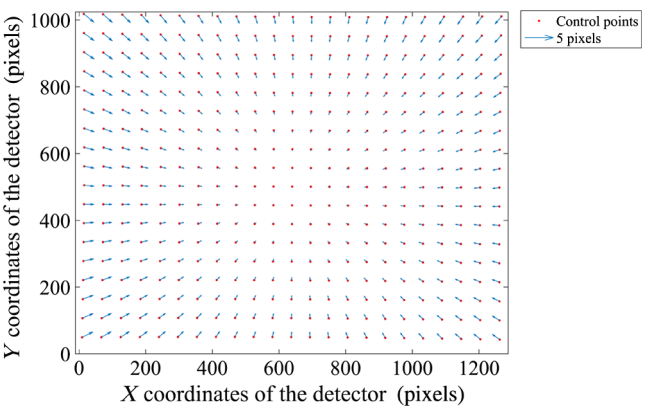

Fig. 7 Distortion vectors for each control point.

In the distortion calibration of the star sensor, the imaging plane is divided into nine equal-size areas, as illustrated in Fig. 8. A quadratic polynomial fitting is applied to the distortion of each region, as shown in Eq. (16). In Table 2, the distortion fitting coefficient of each area is summarized, "zones" denotes one to nine partitions, and $a_1, b_1, c_1, \ldots$ are the parameters of Eq. (16). The residual distortion vector of

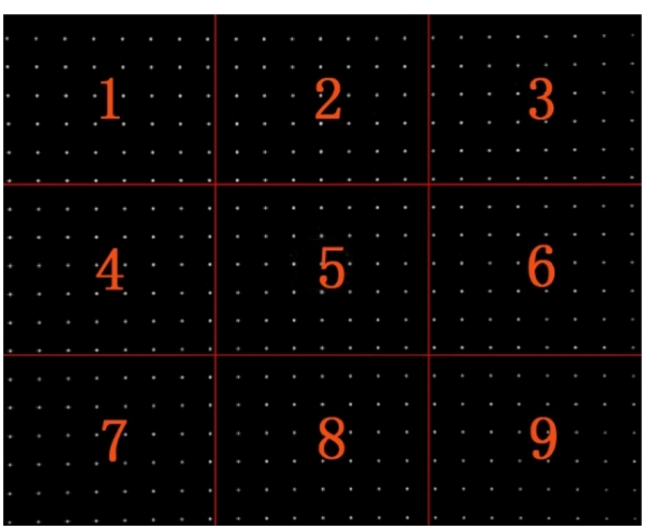

Fig. 8 Partition map of the star sensor focal plane.

Table 2 Quadratic polynomial fitting coefficients of distortion.

Zones	1	2	3	4	5	6	7	8	9
a_1	3.428	2.074	−3.956	3.021	2.532	−6.227	3.047	−0.5773	−7.415
b_1	-9.537×10^{-3}	-4.136×10^{-3}	9.493×10^{-3}	-8.983×10^{-3}	-6.007×10^{-3}	0.01231	-8.252×10^{-3}	-5.872×10^{-4}	1.419×10^{-2}
c_1	-4.660×10^{-3}	-5.227×10^{-3}	-4.385×10^{-3}	-3.485×10^{-3}	-3.951×10^{-3}	-1.154×10^{-4}	-4.048×10^{-3}	2.560×10^{-04}	1.405×10^{-3}
d_1	1.648×10^{-6}	4.591×10^{-6}	4.987×10^{-6}	-6.805×10^{-7}	1.158×10^{-6}	8.463×10^{-7}	-2.657×10^{-7}	-4.073×10^{-6}	-3.483×10^{-6}
e_1	8.723×10^{-6}	2.819×10^{-6}	-5.016×10^{-6}	9.783×10^{-6}	5.148×10^{-6}	-5.619×10^{-6}	8.049×10^{-6}	3.770×10^{-6}	-5.167×10^{-6}
f_1	4.095×10^{-6}	2.360×10^{-6}	-4.405×10^{-7}	3.531×10^{-6}	3.272×10^{-6}	-1.845×10^{-7}	4.060×10^{-6}	2.459×10^{-6}	1.471×10^{-6}
a_2	0.43238	0.2435	−0.7847	0.1421	−1.084	−3.462	−2.657	−4.626	−8.119
b_2	-7.674×10^{-4}	-7.087×10^{-4}	9.689×10^{-4}	-7.592×10^{-4}	1.157×10^{-3}	0.004589	9.138×10^{-4}	0.003608	6.268×10^{-3}
c_2	-3.396×10^{-3}	-2.047×10^{-3}	9.165×10^{-4}	-1.587×10^{-3}	1.634×10^{-3}	5.231×10^{-3}	6.249×10^{-3}	9.559×10^{-3}	1.601×10^{-2}
d_2	4.212×10^{-6}	1.185×10^{-6}	-2.204×10^{-6}	6.292×10^{-6}	2.443×10^{-6}	-3.723×10^{-6}	3.477×10^{-6}	2.297×10^{-6}	-3.726×10^{-6}
e_2	-6.027×10^{-7}	9.513×10^{-8}	-4.571×10^{-7}	-2.141×10^{-6}	-1.929×10^{-6}	-1.959×10^{-6}	-1.398×10^{-6}	-3.935×10^{-6}	-2.704×10^{-6}
f_2	2.973×10^{-6}	3.131×10^{-6}	2.717×10^{-6}	-2.376×10^{-7}	-1.834×10^{-6}	-4.962×10^{-7}	-5.748×10^{-6}	-7.272×10^{-6}	-8.341×10^{-6}

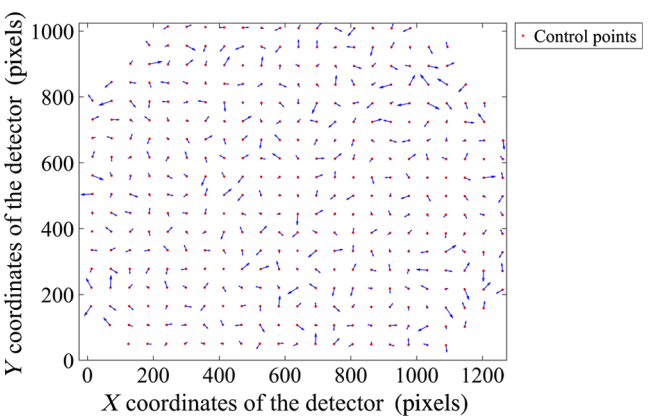

Fig. 9 Residuals for each control point.

each control point is presented in Fig. 9. The maximum residual value is 6.0 arc sec, which can be obtained from Eq. (18).

In the single-star measurement, the relative measurement accuracy of the star sensor calibrated in this study is better than 6 arc sec. In the actual star recognition process, the star sensor will simultaneously measure the positions of multiple navigation stars, which can average the error according to the multistar measurement error formula:

$$E_m = \frac{E_s}{\sqrt{N}}, \tag{19}$$

where N denotes the navigation star and E_s is the single-star measurement error.

The threshold value of the star sensor on an orbit is five navigation stars.[28,29] Therefore, the multistar measurement error caused by the proposed calibration method will be <2.68 arc sec, which meets the requirement of an on-orbit accuracy of 7 arc sec.

4 Conclusion

In this study, the parallel light produced by the diffraction from a 2-D Dammann grating is used to simulate the stars at infinity, to avoid the shortcomings of the static and dynamic calibration methods of star sensors. A procedure to calculate the principal point and principal distance of a star sensor and the tilt angle of incident light using the fitting method is proposed. Partition correction of the distortion of the star sensor optical system is performed using the quadratic polynomial fitting method. Using the calibration system established in this paper, calibration of a nanostar sensor with a focal length of 25 mm and full field of view of 15 deg has been performed. The calibration accuracy of the single-star measurement is better than 6.0 arc sec and the multistar measurement error is <2.68 arc sec, which meets the requirement of high-precision star sensor calibration and verifies the feasibility of the proposed method.

Acknowledgments

We acknowledge the technical staffs of the Optical Design Laboratory of Chang Guang Satellite Technology Co. Ltd. for their equipment. This work was supported by the National Science Foundation for Young Scholars of China (Grant No. 61505203).

References

1. B. Liang et al., "Research status and development tendency of star tracker technique," *Chin. Opt.* **9**(1), 16–29 (2016).
2. S. Zhang et al., "Novel approach to improve the attitude update rate of a star tracker," *Opt. Express* **26**(5), 5164–5181 (2018).
3. M. Yi et al., "Calibration method of high-accuracy star sensor," *Chin. J. Sci. Instrum.* **38**(9), 2154–2160 (2017).
4. H. J. Zhong, M. F. Yang, and X. Lu, "Calibration method of star sensor," *Acta Opt. Sin.* **30**(5), 1343–1348 (2010).
5. G. F. Sun, G. Y. Zhang, and R. Zhang, "Star sensor calibration research and development," *J. Changchun Univ. Sci. Technol.* **33**(4), 8–14 (2010).
6. X. G. Wei et al., "Star sensor calibration based on integrated modelling with intrinsic and extrinsic parameters," *Measurement* **55**, 117–125 (2014).

7. Y. Liu et al., "Machine learning based on-orbit distortion calibration technique for large filed-of-view star tracker," *Infrared Laser Eng.* **45**(12), 282–290 (2016).
8. F. Q. Zhou et al., "Novel autonomous on-orbit calibration method for star sensor," *Opt. Lasers Eng.* **67**, 135–144 (2015).
9. G. F. Sun et al., "Design of very high accuracy star simulator," *Opt. Precision Eng.* **19**(8), 1730–1735 (2011).
10. Y. B. Leng, L. H. Dong, and Y. J. Sun, "Study on 1 × 11 Dammann grating with sub-wavelength structure," *Infrared Laser Eng.* **43**(3), 812–817 (2014).
11. S. H. Yan, *Design of Diffractive Micro-Optics*, National Defense Industry Press, China (2011).
12. M. Bauer et al., "Geometrical camera calibration with diffractive optical elements," *Opt. Express* **16**(25), 20241–20248 (2008).
13. S. Thibault, A. Arfaoui, and P. Desaulniers, "Cross-diffractive optical elements for wide angle geometric camera calibration," *Opt. Lett.* **36**(24), 4770–4772 (2011).
14. A. Arfaoui, S. Thibault, and P. Desaulniers, "Calibration of zoom lens with virtual optical pattern," *Opt. Eng.* **54**(5), 054107 (2015).
15. A. Arfaoui and S. Thibault, "Calibration of aerial and panoramic camera using cross-diffractive optical elements," in *Proc. IEEE Int. Instrum. and Meas. Technol. Conf.*, IEEE (2012).
16. A. Hermerschmidt, S. Krüger, and G. Wernicke, "Binary diffractive beam splitters with arbitrary diffraction angles," *Opt. Lett.* **32**(5), 448–450 (2007).
17. R. C. McPhedran, G. H. Derrick, and L. C. Brown, "Theory of crossed gratings," in *Electromagnetic Theory of Gratings*, R. Petit, Ed., pp. 227–276, Springer-Verlag, Berlin, Heidelberg (1980).
18. P. Xi et al., "Design and fabrication of 64 × 64 spot array Dammann grating," *Chin. J. Lasers* **28**(4), 369–371 (2001).
19. P. Y. Qiao et al., "Calibration of high-accuracy star sensor," *Infrared Laser Eng.* **41**(10), 2779–2784 (2012).
20. H. Zhang et al., "Parameter calibration and error compensation of star sensor," *Opto-Electron. Eng.* **32**(9), 1–4 (2005).
21. J. P. He et al., "Calibration method for wide field of view star sensor," *Acta Opt. Sin.* **31**(10), 1023001 (2011).
22. W. C. Lin, "Structure design and calibration of high-accuracy star sensor," *J. Changchun Univ. Sci. Technol.* **27**(6), 51–54 (2014).
23. J. Y. Lu et al., "Improved design of splitters," *Opt. Precision Eng.* **11**(6), 572–575 (2003).
24. Y. L. Yuan, Y. Zheng, and L. Du, "High-accuracy centroid algorithm of star points," *J. Geomatics Sci. Technol.* **29**(2), 122–126 (2012).
25. X. D. Hu et al., "Method of star centroid extraction used in daytime star sensors," *J. Chin. Inertial Technol.* **22**(4), 481–485 (2014).
26. M. S. Wei, F. Xing, and Z. You, "A real-time detection and positioning method for small and weak targets using a 1D morphology-based approach in 2D images," *Light Sci. Appl.* **7**, 18006 (2018).
27. W. J. Wang et al., "Noise suppression algorithm of short-wave infrared star image for daytime star sensor," *Infrared Phys. Technol.* **85**, 382–394 (2017).
28. X. Zhong et al., "Focal plane assembly and calibrating of CMOS star sensor," *Opto-Electron. Eng.* **38**(9), 1–5 (2011).
29. J. Li, *Research and Implementation of Star Sensor*, Jilin People's Publishing House, China (2008).

Kun Zhang studied optical system design and thermal stability optimization of the star sensor at Changchun Institute of Optics, Fine Mechanics and Physics, Chinese Academy of Sciences. During the period of studying for his master's degree, he engaged in various lens design, such as fish-eye lens, zoom optical system, panoramic annular lens, and off-axis three-mirror system. Currently, he is studying for his doctor's degree at the University of Chinese Academy of Sciences.

Xing Zhong received his PhD with major in optical engineering and worked at CIOMP as an associate professor, during 2009 to 2014. In 2015, he became a full professor at CIOMP and took part in the work for founding Chang Guang Satellite Technology Co. Ltd. (CGSTL). Currently, he is the chief engineer of CGSTL and also a professor at the University of Chinese Academy of Sciences.

Wei Wang majored in optical engineering at Changchun Institute of Optics, Fine Mechanics and Physics, Chinese Academy of Sciences. He joined aspheric on for his master's thesis in the Design Department. In the scope of his master's thesis, he designed the specific structure of Dammann grating. In addition, he analyzed the diffraction and the intensity distribution of Dammann grating. Currently, he is studying for his doctor's degree at the University of Chinese Academy of Sciences.

Yao Meng majored in instrument science and technology during 2013 to 2017. In 2017, he received his PhD from Changchun University of Science and Technology. When he graduated, he took part in the work for founding CGSTL. Currently, he is studying the design of space optical system in CGSTL.

Chi Ma majored in optical engineering at Harbin Industrial University and received his master's degree in 2015. In 2016, he worked at CGSTL and until now he is still mainly engaged in space optical system design and optical testing.